Supplementary Materials

A deep neural network potential model for transition metal diborides

Fu-Zhi Dai[1,2], Bo Wen[3,*], Yixuan Hu[4], Xin-Fu Gu[1,*]

[1]School of Materials Science and Engineering, University of Science and Technology Beijing, Beijing 100083, China.
[2]AI for Science Institute, Beijing 100084, China.
[3]Science and Technology on Advanced Functional Composite Laboratory, Aerospace Research Institute of Materials and Processing Technology, Beijing 100076, China.
[4]School of Materials Science and Engineering, Shanghai Jiao Tong University, Shanghai 200240, China.

*Correspondence to: Dr. Bo Wen, Science and Technology on Advanced Functional Composite Laboratory, Aerospace Research Institute of Materials & Processing Technology, South Dahongmen Road 1#, Beijing 100076, China. E-mail: BHVeen@163.com; Prof. Xin-Fu Gu, School of Materials Science and Engineering, University of Science and Technology Beijing, Xueyuan Road 30#, Beijing 100083, China. E-mail: xinfugu@ustb.edu.cn

Supplementary Text 1. Crystal structure of transition metal diborides (TMB$_2$)

Transition metal diborides (TMB$_2$) crystalize to AlB$_2$-like structure with the space group of P6/mmm, stacking alternatively by close-packed TM layers and graphite-like hexagonal B layers, as illustrated in Supplementary Figure 1. TM atoms and boron atoms are respectively located at 1a (0, 0, 0) and 2d (1/3, 2/3, 1/2) Wyckoff positions.
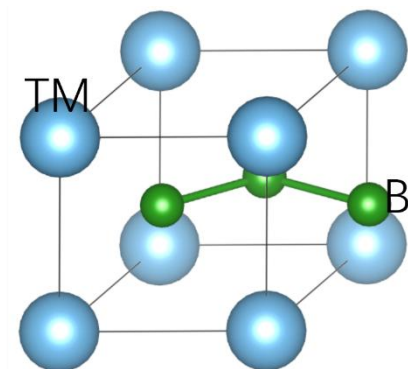
Supplementary Figure 1. Schematic illustration on the crystal structure of transition metal diboride. The big spheres are transition metals, while the small spheres represent boron.
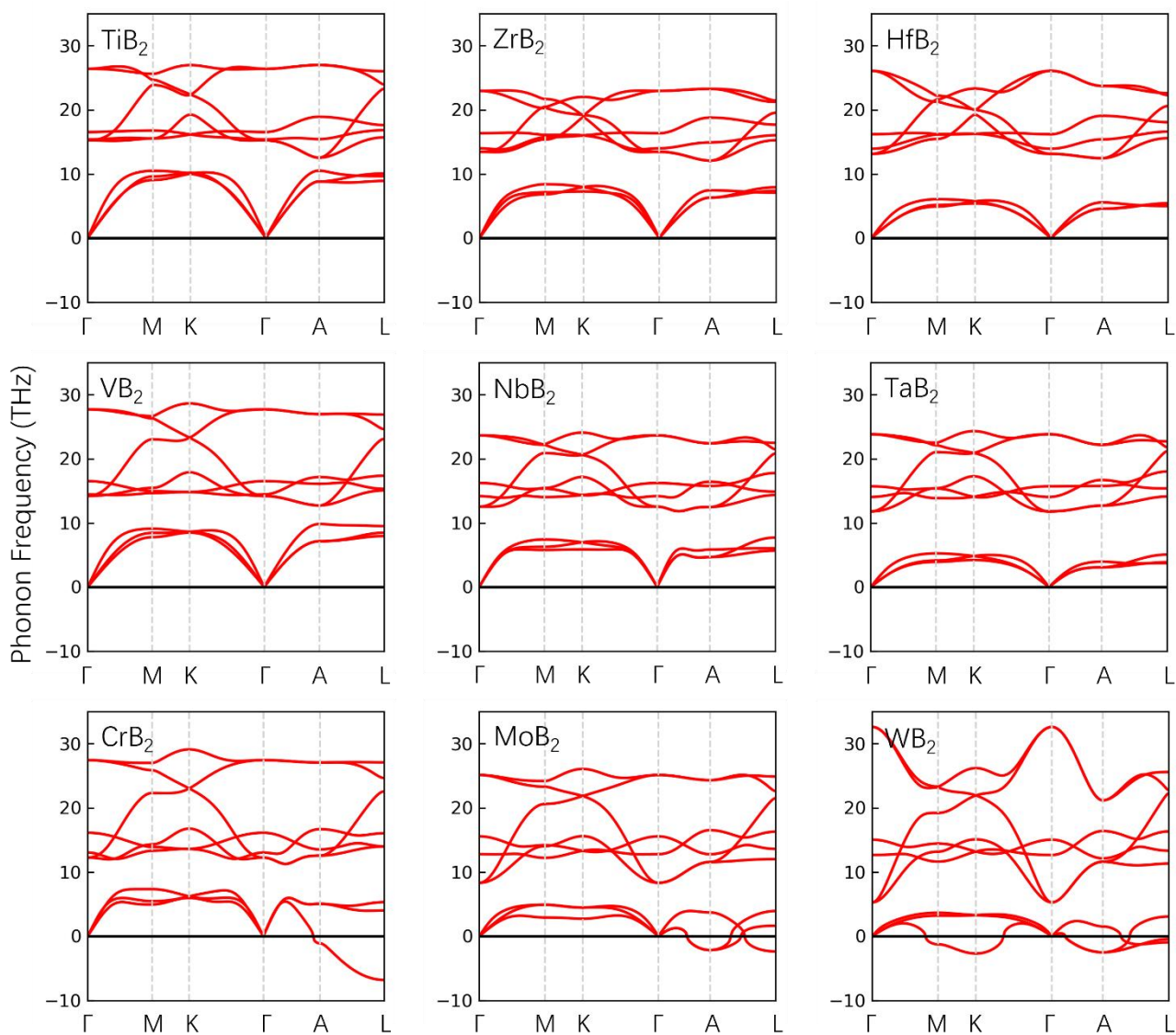
Supplementary Figure 2. Phonon dispersion curves of TMB$_2$s.

Supplementary Table 1. Melting points (in K) measured by experiments (exp), calculated by the DP model (cal) or averaged from constitute mono-compounds (ave). Experimental data are from ref[1]

	exp	cal	ave
TiB_2	3,498	3,537	
ZrB_2	3,518	3,430	
HfB_2	3,653	3,564	
VB_2		3,057	
NbB_2	3,309	3,202	
TaB_2	3,310	3,143	
CrB_2		2,298	
MoB_2		2,455	
WB_2		2,323	
$Zr_{0.25}Hf_{0.25}Nb_{0.25}Ta_{0.25}B_2$		3,332	3,335
$Ti_{0.2}Zr_{0.2}Hf_{0.2}Nb_{0.2}Ta_{0.2}B_2$		3,370	3,375
$V_{0.2}Zr_{0.2}Hf_{0.2}Nb_{0.2}Ta_{0.2}B_2$		3,192	3,280
$W_{0.2}Zr_{0.2}Hf_{0.2}Nb_{0.2}Ta_{0.2}B_2$		3,135	3,133

Supplementary Text 2. Method on the construction of grain boundaries

Symmetric tilt grain boundaries are constructed based on coincident site lattice (CSL) theory, which are similar to our previous work[2]. When exact CSL cannot be defined, small elastic strains should be applied to the system. The tilt axes are [010] and [210] of diboride, respectively. Supplementary Figure 3 takes the 010_21 grain boundary as an example to illustrate how a grain boundary is defined. A grain boundary plane can be defined by two in-plane vectors, which are contained in its name. One is the rotation axis of the symmetric tilt grain boundary. The other is a combination of other two basis vectors. For example, the 010_21 grain boundary has a rotation axis of [010] and another in-plane direction of 2[001]+[$\overline{2}\overline{1}$0], i.e., [$\overline{2}\overline{1}$2], while the 210_12 grain boundary has a rotation axis of [210] and another in-plane direction of [001]+2[010]. Supplementary Table 1 lists the crystallographic features of the fourteen grain boundaries.
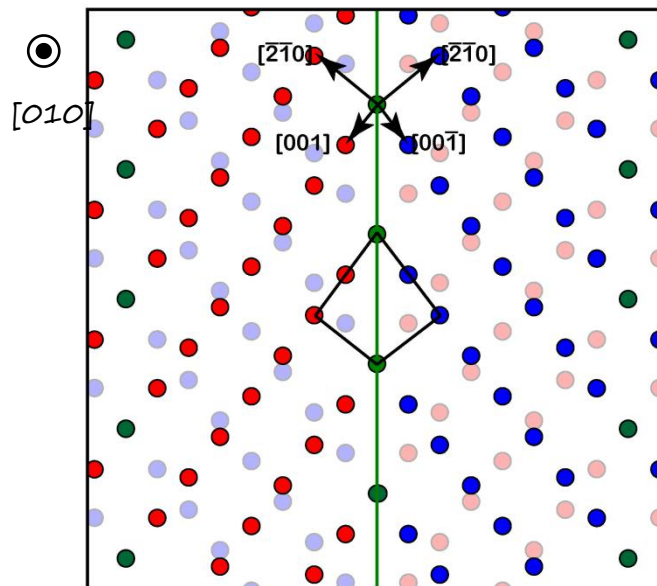
Supplementary Figure 3. Illustration on the definition of 010_21 grain boundary. Red points represent one diboride lattice comprising the grain boundary, while blue points represent the other diboride lattice. Green points defines the CSL points.

Supplementary Table 2. Crystallographic information of symmetric tilt grain boundaries studied in this work. The four-index representation of the vectors are also listed for better understanding

	11	12	13	21	23	31	32
[010] [$\bar{1}2\bar{1}0$]/3	$[\bar{2}\bar{1}1]$ $[\bar{1}011]$	$[\bar{4}\bar{2}1]$ $[\bar{2}021]$	$[\bar{6}\bar{3}1]$ $[\bar{3}031]$	$[\bar{2}\bar{1}2]$ $[\bar{1}012]$	$[\bar{2}\bar{1}3]$ $[\bar{1}013]$	$[\bar{4}\bar{2}3]$ $[\bar{2}023]$	$[\bar{6}\bar{3}2]$ $[\bar{3}032]$
	$[\bar{2}\bar{1}\bar{1}]$ $[\bar{1}01\bar{1}]$	$[\bar{4}\bar{2}\bar{1}]$ $[\bar{2}02\bar{1}]$	$[\bar{6}\bar{3}\bar{1}]$ $[\bar{3}03\bar{1}]$	$[\bar{2}\bar{1}\bar{2}]$ $[\bar{1}01\bar{2}]$	$[\bar{2}\bar{1}\bar{3}]$ $[\bar{1}01\bar{3}]$	$[\bar{4}\bar{2}\bar{3}]$ $[\bar{2}02\bar{3}]$	$[\bar{6}\bar{3}\bar{2}]$ $[\bar{3}03\bar{2}]$
[210] [$10\bar{1}0$]	$[011]$ $[\bar{1}2\bar{1}3]$/3	$[021]$ $[\bar{2}4\bar{2}3]$/3	$[031]$ $[\bar{1}2\bar{1}1]$	$[012]$ $[\bar{1}2\bar{1}6]$/3	$[023]$ $[\bar{2}4\bar{2}9]$/3	$[013]$ $[\bar{1}2\bar{1}9]$/3	$[032]$ $[\bar{1}2\bar{1}2]$
	$[01\bar{1}]$ $[\bar{1}2\bar{1}3]$/3	$[02\bar{1}]$ $[\bar{2}4\bar{2}3]$/3	$[03\bar{1}]$ $[\bar{1}2\bar{1}\bar{1}]$	$[01\bar{2}]$ $[\bar{1}2\bar{1}6]$/3	$[02\bar{3}]$ $[\bar{2}4\bar{2}9]$/3	$[01\bar{3}]$ $[\bar{1}2\bar{1}9]$/3	$[03\bar{2}]$ $[\bar{1}2\bar{1}\bar{2}]$

[010] and [210] are tilt axis.

Basis vectors of [010] tilt grain boundaries are [001] and [$\bar{2}\bar{1}0$] for one crystal, [$00\bar{1}$] and [$\bar{2}\bar{1}0$] for the other crystal; while basis vectors of [210] tilt grain boundaries are [001] and [010] for one crystal, [$00\bar{1}$] and [010] for the other crystal.

The headlines means linear combination of basis vectors to define CSL vectors, e.g., 21 of [010] tilt grain boundary means a CSL vector in the grain boundary plane is linear combination of two [001] basis vector and one [$\bar{2}\bar{1}0$] basis vector, i.e., [$\bar{2}\bar{1}2$].
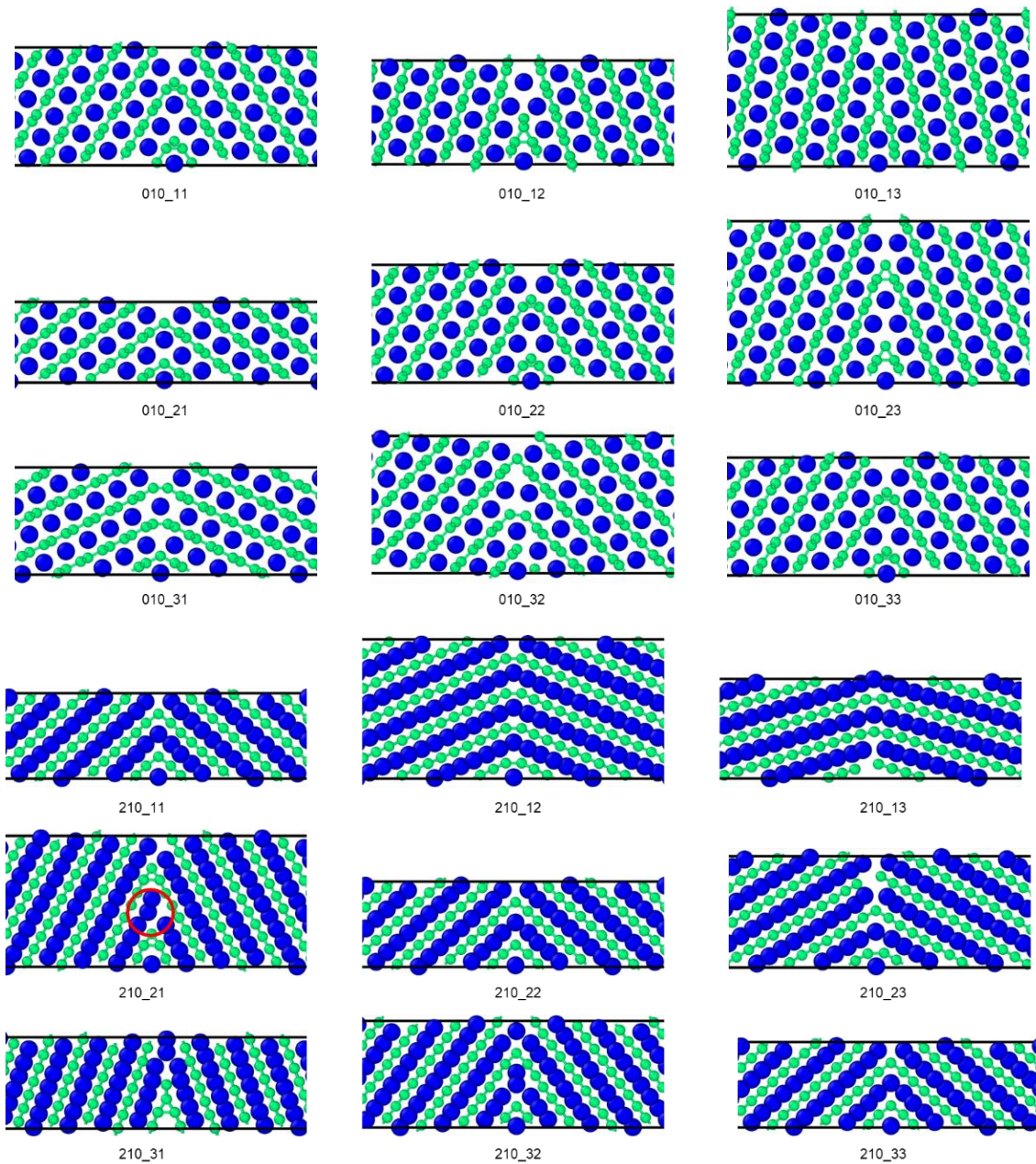
Supplementary Figure 4. Relaxed atomic structures for the grain boundaries studied in this work. 010_22, and 010_33 are the same as 010_11 grain boundary, while 210_22, and 210_33 are the same as 210_11 grain boundary. In the 210_21 grain boundary, a circle indicates the presence of local free volume, potentially accommodating additional atoms. Green atoms are boron, and blue atoms are metals. When drawing B-B bonds, the criterion is set to be 2 Å.

Supplementary Table 3. Ideal strength (in GPa) of grain boundaries. Without_MC means the metallic sites are randomly occupied, while with_MC means the last snapshot after MC/MD simulation is adopted for tensile simulation. Without_W means no W is added, while with_W means 5 at% W is added into metallic sites

	ZrB_2		$Ti_{1/3}Zr_{1/3}Hf_{1/3}B_2$ (ME-TMB$_2$)			
	Without_W	With_MC With_W	Without_MC Without_W	With_MC Without_W	Without_MC With_W	With_MC With_W
100_11	14.9	20.3	16.5	16.6	16.2	20.3
100_12	13.4	16.6	13.3	18.3	14.0	17.6
100_13	16.2	15.7	17.1	19.8	18.0	19.3
100_21	17.4	24.7	18.3	20.0	17.9	24.6
100_23	14.3	19.4	16.5	19.3	16.7	18.6
100_31	19.5	18.2	22.9	23.0	18.8	24.5
100_32	12.0	13.7	13.2	14.3	11.9	15.6
210_11	15.2	21.6	17.9	17.5	17.0	22.1
210_12	15.4	17.7	17.9	18.1	19.2	17.4
210_13	12.2	16.3	12.6	17.1	14.2	17.3
210_21	17.2	16.4	17.6	17.8	16.0	18.8
210_23	11.6	14.9	14.2	13.3	14.7	16.6
210_31	12.1	15.4	12.8	16.4	12.1	15.3
210_32	13.0	17.9	14.1	15.4	11.7	18.6

During tensile simulation, stress variation is approximately 1 GPa in the tensile direction. Consequently, when the strength difference is less than 1 GPa, distinguishing which grain boundary is stronger becomes inconclusive due to the margin of error.

Supplementary Text 3. The predictive capabilities of the DP model on grain boundary energies and grain boundary segregation energies.

In this section, we illustrate the predictive capabilities of the DP model on grain boundaries by examining the grain boundary energies and grain boundary segregation energies, and comparing the results to DFT calculations. Owing to the computational limitations of DFT, analyses are constrained to small supercells. We chose the 010_21 and 210_11 grain boundaries for this study, depicted in Supplementary Figure 5A and B, respectively. Notably, the 010_21 structure here deviates from that shown in Supplementary Figure 4. To ascertain the grain boundary energy accurately, it is requisite to construct a supercell that mirrors the bulk phase's chemical composition, maintaining a 1:2 metal-to-boron ratio. Consequently, we refrain from removing boron atoms adjacent to the grain boundary (highlighted by an ellipse), a decision that leads to pronounced distortion of the boron framework, as evident from Supplementary Figure 5A.

The calculated grain boundary energies of TMB_2 compounds (TM = Ti, Zr, Hf, V, Nb, Ta, Cr, Mo, W) using both the DP model and DFT are shown for comparison in Supplementary Table 4. The accuracy for TiB_2, ZrB_2, and HfB_2 is found to be high, moderate for VB_2, NbB_2, and TaB_2, and low for CrB_2, MoB_2, and WB_2. However, the trend of grain boundary energy variation with the transition metal is correctly captured. In TiB_2, ZrB_2, and HfB_2, the grain boundaries possess high energy; in VB_2, NbB_2, and TaB_2, medium energy; and in CrB_2, MoB_2, and WB_2, low energy. Notably, the DFT-computed grain boundary energies for WB_2 are negative, highlighting its inherent instability. Moreover, very low grain boundary energies are also observed for CrB_2 and MoB_2, suggesting a predisposition of Cr, Mo, and W to segregate at the grain boundaries due to favorable local atomic structures.

Segregation energies were also computed for various solutes (Ti, Zr, Hf, V, Nb, Ta, Cr, Mo, W) within TiB_2, ZrB_2, and HfB_2 grain boundaries. Solute insertion sites are marked by arrows in Supplementary Figure 5A and B, with the supercells featuring solute atoms at grain boundary sites (highlighted by a blue arrow) as the reference state. The difference in energy between this state and the reference state defines segregation energy. Supplementary Figure 5C presents a comparison of segregation energies derived from both the DP model and DFT calculations, demonstrating a good correspondence.

When generating the training data for the DP model, no grain boundary structure is included. Nevertheless, as shown by the grain boundary energies and segregation energies, the predictive capabilities of the DP model on grain boundaries are reasonable.

Supplementary Table 4. Comparison of grain boundary energies (meV/Å^2) calculated by the DP model and DFT calculations

		TiB$_2$	ZrB$_2$	HfB$_2$	VB$_2$	NbB$_2$	TaB$_2$	CrB$_2$	MoB$_2$	WB$_2$
010_21	DFT	256	174	191	188	112	91	82	10	-52
	DP	207	141	156	188	134	123	100	84	33
210_11	DFT	140	142	143	67	54	34	13	3	-29
	DP	156	151	155	115	103	88	62	38	6
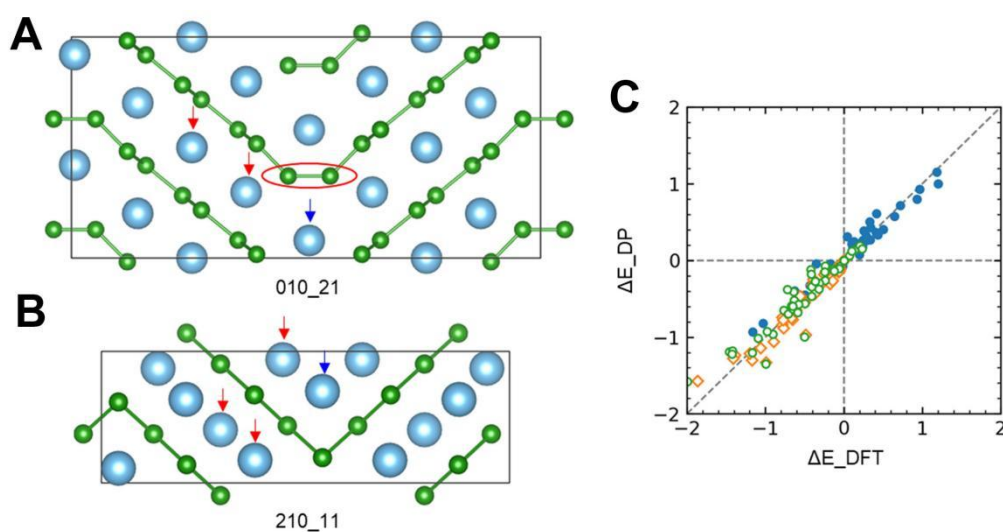
Supplementary Figure 5. Atomic structures of (A) the 010_21 grain boundary and (B) the 210_11 grain boundary constructed for the assessment of grain boundary energy and segregation energy; (C) Segregation energy (ΔE) comparisons between DFT calculations and the DP model. The matrix for blue, orange and green points is TiB$_2$, ZrB$_2$, HfB$_2$, respectively.

References

[1] Rudy E, Harmon DP. Ternary phase equilibria in transition metal-boron-carbon-silicon systems. Part V. compendium of phase diagram data. Tech. Rep. AFML-TR-65-2, Part V, Air Force Materials Lab., Air Force Systems Command, Wright-Patterson Air Force Base, OH, 1969: 5.

[2] Dai FZ, Wen B, Xiang H, Zhou Y. Grain boundary strengthening in ZrB$_2$ by segregation of W: atomistic simulations with deep learning potential. *J Eur Ceram Soc* 2020;40:5029-36. [DOI: 10.1016/j.jeurceramsoc.2020.06.007]